ISSN: 2633-4828 Vol. 3 No.1, June, 2021

International Journal of Applied Engineering & Technology

INFLUENCE OF SB ON THE STRUCTURAL, MICROSTRUCTURAL, OPTICAL PROPERTIES OF OXYGEN-DEFICIENT SNO_2

Rita Singh[1] and Jitesh Kumar[2,*]

[1]Department of Physics, ARSD College, University of Delhi-110021, India,

[2]Department of Physics and Electronics, Rajdhani College, University of Delhi-110015, India,

ABSTRACT

$Sn_{1-x}Sb_xO_{2-\delta}$(x = 0.0, 0.1, 0.2, 0.3) bulk samples were synthesized via a solid-state reaction route. The X-ray diffraction patterns show that the overall structure/phase remains unchanged with antimony (Sn) substitution up to x = 0.3 SEM examination reveals larger grain sizes and increased pores/voids between grains in Sb doped SnO_2 samples. TEM images indicate undoped SnO_2 grains with diameters ranging from 25 to 120 nm, mostly in cubic or spherical shapes and transform into microcubes/spheres with increasing antimony content. Reflectance increases, while absorbance decreases in the UV-vis spectra of $Sn_{1-x}Sb_xO_{2-\delta}$ samples with higher antimony concentrations (Sb) within the 0.36 – 0.8 μm wavelength range. The energy bandgap of Sb doped SnO_2 samples, obtained from UV-Vis absorption spectroscopy, increases from 3.367 eV to 3.558 eV with rising Sbconcentration.

1. INTRODUCTION

Metal oxides hold significant importance across various domains of physical sciences [1]. These compounds possess distinctive attributes encompassing captivating electronic and magnetic characteristics, spanning from metallic and semiconducting behaviours to superconductivity, insulation, and various forms of magnetism. These oxides are affluent for numerous device applications in oxygen generators, corrosion-resistant coatings, fuel cells, organic synthesis, including the manufacture of microelectronic circuits, capacitors, sensors, piezoelectric devices, semiconductors, engineered ceramics production, and catalysts, serving as both a support and active component. Among the existing metal oxides, tin(IV) dioxide (SnO_2)stands out as a significant member, having undergone extensive investigation due to its versatility in a wide array of applications [1-3]. These applications include its use in gas sensors, catalytic processes, far-infrared dichromic mirrors and transparent conductive oxides.Tin (IV) dioxide's importance lies in its chemical and thermal stability, inherent non-stoichiometry, optical transparency, and the ability to modulate conductivity across a broad spectrum, all of which render it highly suitable for the aforementioned purposes [4].

Possessing tetragonal rutile structure with space group $P4_2/mnm$, a wide bandgap degenerate semiconductor, SnO_2 has a direct band gap of about 3.6 eV in the ultra-violet region. For many technological applications, it is an important feature of SnO_2[1, 8]. In its stoichiometric state, SnO_2 functions as an insulator; however, when it exists with oxygen deficiency, tin dioxide exhibits characteristics of an n-type semiconductor [3]. This oxygen deficiency can result from either the presence of oxygen vacancies or the insertion of tin interstitials. This process of oxygen vacancy generation may involve the conversion of certain *Sn* (IV) ions to *Sn* (II), potentially acting as a mechanism for the charge compensation [5]. Nevertheless, the intricate electronic structure associated with defects within the materials has yet to receive comprehensive scrutiny. The electronic conductivity could be attributed to the mobility of electrons transitioning from *Sn* (II) sites to *Sn* (IV) sites [5].

In this paper we report the influence of Sb doping on structural, Microstructural, optical properties of oxygen deficient $Sn_{1-x}Sb_xO_2$ samples with x = 0.0, 0.1, 0.2, 0.3 synthesized via conventional solid-state ceramic route. In this current investigation, we explored the utilization of SnO_2 with Sb^{5+} substitutions,delving into their potential applications. This study will help in optimization of the composition for better performance of HECs. Further, the earlier works are reported at low temperature single step sintering of SnO_2. The present study employsthe two-step sintering for achieving high oxygen deficiency by regulating sample phase homogeneity, element composition, and morphology. This study will support that oxygen deficient oxides are superior compared to polymer-based sensors for humidity sensing performance.

2. EXPERIMENTAL DETAILS

We used conventional solid state reaction method to synthesize undoped and *Sb* doped SnO_2 samples. The metallic tin (purity 99.99, Sigma Aldrich) and Sb_2O_5 (99.99% Aldrich Chemical) were used as starting materials. The bulk SnO_2 was synthesized by oxidizing the metallic tin (purity 99.99, Aldrich) at 700°C for 8 hour in air. The thermal oxidation of metallic tin powder is expressed as:

$$Sn_{(s)} + 1/2\, O_{2(g)} \rightarrow SnO_{(v)}$$
$$SnO_{(v)} + 1/2\, O_{2(g)} \rightarrow SnO_{2\,(s)} \quad (1)$$

These calcined powders of undoped SnO_2 were taken as the starting materials for the preparingof undoped and *Sb*-doped SnO_2 samples. The Sb-doped SnO_2 powders ($Sn_{1-x}Sb_xO_2$ where x = 0,0.1, 0.2& 0.3) were prepared by mixing undoped SnO_2 with Sb_2O_5 as per the stoichiometry. The mixed powders were calcined in alumina crucible at 700°C for 15 hour. The pellets for undoped and Sb-doped SnO_2 fine powder was pressed into 2 mm-thick pellets with circular shape of 10 mmin diameter using PVA (polyvinyl alcohol) as a binder. Finally, pellets of $Sn_{1-x}Sb_xO_2$ (x = 0, 0.1, 0.2 & 0.3) samples were sintered in air at 900°C for 9 hours and 1300°C for 16 hours respectively.

The structure and phase purity of the $Sn_{1-x}Sb_xO_2$ (x = 0, 0.1, 0.2 & 0.3) samples ground from circular pellets were examined by powder diffraction studies using X-ray powder diffractometer (18 KW Rigaku, Japan) with *Cu-Kα* radiation (λ = 1.5418 Å) at room temperature. The surface morphology of undoped and *Sb* doped SnO_2 samples was carried out at 25 kV, with a resolution of 3.5 nm, by a JSM-5600(JoelScanning Electron Microscope) operated. The structural/Microstructural characteristics of undoped and *Sb*-doped SnO_2 samples were made explored by TEM (transmission electron microscope) (FEI Tecnai G220) in both the imaging and diffraction modes. Optical studies were carried out for undoped and Sb-doped *SnO2* samples by measuring the reflectance in the range 0.2-0.8 μm at ambient temperature using (Varian Cary 500) UV-Vis spectrophotometer. The undoped and Sb-doped *SnO2* powder samples were made into rectangular pellets of area 0.91cm^2 and sintered at 700 °C for 4 hours.

3. RESULTS AND DISCUSSION

3.1 X-RAY DIFFRACTION MEASUREMENTS

The X-ray diffraction spectra of $Sn_{1-x}Sb_xO_2$ (x = 0, 0.1, 0.2 & 0.3) samples is shown in Figure 1.The indexing of the peaks in the diffraction spectra is on the basis of tetragonal rutile phase oftin oxide (JCPDS # 41-1445). It can be observed from the diffraction spectra that all the peaksof all $Sn_{1-x}Sb_xO_2$ (x = 0, 0.1, 0.2 & 0.3) samples matches well with rutile phase of *SnO* andconfirms the formation of space Group *P42/mnm.* The XRD patterns doesn't display any reflection peaks from impurities, for example unreacted *Sn, Sb* or other oxide phases of Sb_2O_5 or Sb_2O_3, and indicate high phase purity in the samples. The XRD spectra display unusual variation of peak broadening and shifting with Sb doping. For x=0.1 ($Sn_{0.9}Sb_{0.1}O_2$), the XRD peaks broadens and shift to higher 2θ as compared to SnO_2 suggesting a lattice compression with lower crystallite size as compared to SnO_2 . With further introduction of Sb at x=0.2and 0.3, the XRD peak intensity decreases with sharpened peaks and shifting to lower 2θ withrespect to both SnO_2 and $Sn_{0.9}Sb_{0.1}O_2$. This change in XRD spectra indicates a higher crystallitesize and lattice expansion in the samples. Table 1 displays crystallite size of $Sn_{1-x}Sb_xO_2$ (x = 0.0, 0.1, 0.2 & 0.3) samples obtained using Debye-Scherer's equation [11]

$$D = k.\lambda/(\beta \cos\theta) \quad (2)$$

where λ is the x-ray wavelength (1.542 Å for Cu-Kα), θ is the Bragg angle and β is the full FWHM of the diffraction line. The variation observed inthe computed crystallite size corroborates the diffusion phenomena. The initial decrease in thecrystallite size with Sb doping could be due to the decrease in the diffusion rate as a result of *Sb* atoms occupying the crystal boundary positions and hindering the growth of the crystal.

TABLE 1 : LATTICE PARAMETERS OF $Sn_{1-x}Sb_xO_{2-\Delta}$ (X = 0.0, 0.1, 0.2, 0.3)

Composition of Sb(x) in $Sn_{1-x}Sb_xO_{2-\delta}$	Average Crystallite Size (nm)	Lattice parameters	
		a=b (Å)	c (Å)
x=0.0	57	4.7346	3.1787
x=0.1	28	4.7354	3.1822
x=0.2	65	4.7360	3.1843
x=0.3	77	4.7365	3.1899

However, with further increase in *Sb* concentration, the Sb atoms tend to occupy the lattice sites and result in the expansion. This is due to the difference in ionic radii of Sn^{4+}(0.72Å) and Sb^{5+}(0.90Å) ions possibly. This theory is

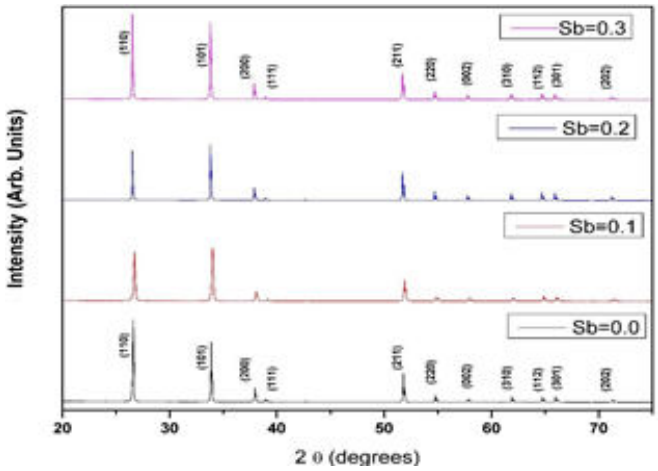

Figure 1: X-Ray Powder Diffraction Patterns of $Sn_{1-X}sb_xo_{2-\Delta}$ System With X = 0.0, 0.1, 0.2, 0.3.

supported with the lattice parameter calculations also tabulated in Table 1. The variation in the crystallite size and lattice parameterscould be understood on the basis of growth mechanism. For low values of *Sb* doping (x = 0.1) in SnO_2, the growth along (101) and (200) directions in SnO_2 are promoted leading to decreasein lattice parameter. However, for higher concentration of *Sb* (x > 0.1), a percolation limit is reached and the preferred growth direction is still (110) direction in SnO_2. This surface of rutileSnO_2 structure has a greater surface energy than (001) surface, so general preferred growth direction of SnO_2 nanospheres in the (001) direction.

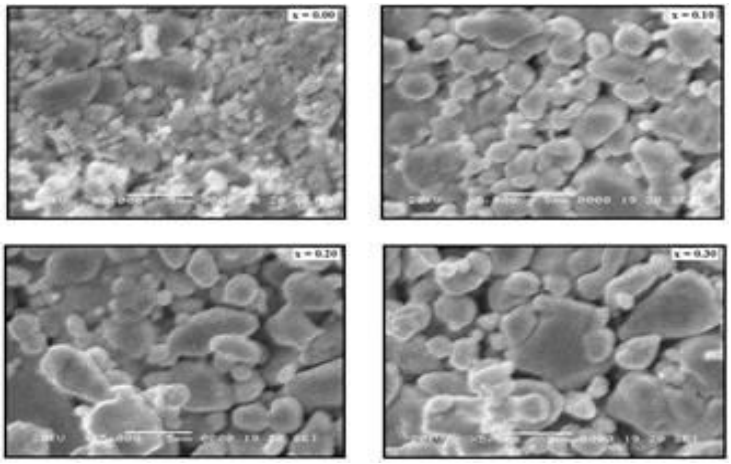

Figure 2: Sem of the Surface of the Bulk $Sn_{1-X}sb_xo_{2-\Delta}$ System With X = 0.0, 0.1, 0.2, 0.3.

3.2 ECANNING ELECTRON MICROSCOPY (SEM)

Figure 2 displays scanning electron micrographs (SEM) of Sb-substituted SnO_2 samples. Pure SnO_2 SEM images reveal uniform grain size with high packing density. Increasing Sb_2O_3 concentration enhances grain uniformity, approaching near homogeneity. Introducing 0.10% *Sb* to SnO_2 results in visible pores amid well-connected grains. Pores/voids increase with *Sb* concentration up to 0.30%. SEM images vividly illustrate the correlation between *Sb* doping and SnO_2 grain size enlargement. The surface morphology of randomly aligned pure and antimony-doped SnO_2 is approximately 100 nm.

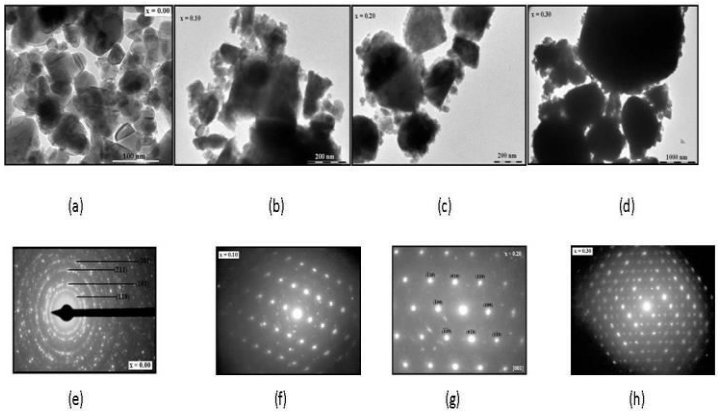

Figure 3(A-D): Transmission Electron Micrograph of the Bulk $Sn_{1-X}sb_xo_{2-\Delta}$ System With X = 0.00, 0.10, 0.20, 0.30 Showing Several Nanocubes Or Nanospheres. (E-H) Selected Area Is Electron Diffraction (Saed) Pattern Corresponding To Fig. 3(A-D) Along [001] Direction.

3.3 TRANSMISSION ELECTRON MICROSCOPY (TEM)

Fig. 3 shows the TEM micrographs and corresponding SAED (Selected Area Electron Diffraction) patterns for *Sb* doped SnO_2 samples. TEM image hints the SnO_2 grains could have size ranging from 25 to 120 mm in diameter and the shape of the most of the grains is spherical or cubic. In the same fig., The SAED pattern of pure SnO_2 sample implies several sharp rings, indexed to the (110), (101), (211), and (301) planes of the rutile crystalline structure of SnO_2 (JCPDS card no. 041-1445). The TEM micrographs of *Sb*-doped SnO_2 show that the grain size increases (from nano to micro) as the *Sb* concentration rises, and that regular SAED patterns are produced, which point to an increase in lattice parameters due to doping [11].

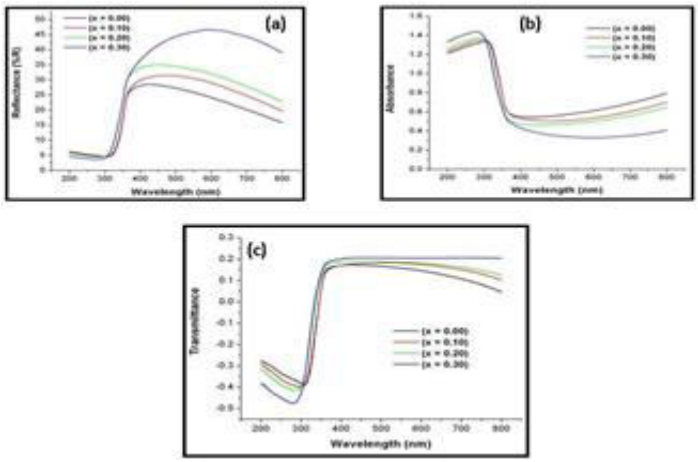

Figure 4: Uv-Vis Reflectance, Absorbance and Transmittence Spectra of $Sn_{1-X}sb_xo_{2-\Delta}$ System with X=0.0, 0.1, 0.2, 0.3

3.4 UV-Vis SPECTROSCOPY

The $Sn_{1-x}Sb_xO_{2-\delta}$ (x = 0.0, 0.1, 0.2, 0.3) sample's optical reflectance spectra as a function wavelength spanning 200 to 800 nm are displayed in Figure 4(a). All *Sb*-doped SnO_2 (x = 0.0, 0.1, 0.2, 0.3) have low reflectance up to a wavelength of 300 nm, but it increases beyond that point. The absorbance of light in Figure 4(b) illustrates the spectra of the $Sn_{1-x}Sb_xO_{2-\delta}$ samples at various *Sb* concentrations (x = 0.0, 0.1, 0.2, 0.3). The figure indicates that as the doping concentration increases, the absorbance increases for the range of 200–310 nm and decreases for the range of 365–800 nm. Using the reflectance (Figure 4(a)) and absorbance (Figure 4(b)) spectra, the transmittance of the synthesized samples was determined by the relation:

$$T = 1 - (R + A) \qquad (3)$$

where, *T, R and A* are Transmittance, Reflectance, and Absorbance respectively. Figure 4(c) reveals the transmittance spectra (derived from (3)) for the bulk $Sn_{1-x}Sb_xO_{2-\delta}$ (x = 0.0, 0.1, 0.2, 0.3) samples in the 200 – 800 nm range.

The figure makes this very evident: at wavelengths between 355 and 800 nm, Sb doping increases transmittance, while at wavelengths below 300 nm, transmittance decreases. When Sb doping is added, the transmittance usually decreases and the reflectance rises as a result. This pattern is frequently seen in semiconductors that have been doped with metal.

Using the absorbance data from *Sb* doped SnO_2; the plot of the optical absorption coefficient α versus photon energy *hv* was obtained and is shown in Figure (5). The absorption coefficient α expressed as function of the incident energy [12] is

$$\alpha = {}^{A}/_{hv}\ (hv - E_g)^n \qquad (4)$$

Eqn. (4) illustrates how α varies with photon energy.

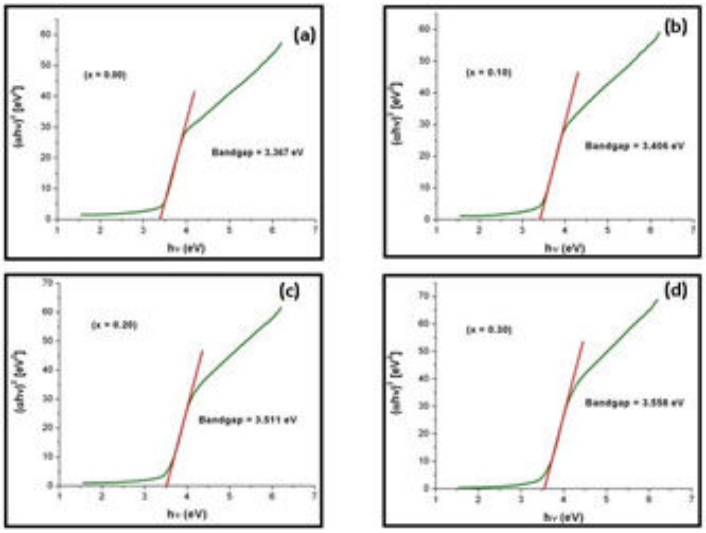

Figure 5: $(Ahv)^2$ Vs Photon Energy (Hv)Curve For The Bulk $Sn_{1-X}sb_xo_{2-\Delta}$ System With X = 0.0, 0.1, 0.2 And 0.3.The Extrapolation A = 0 Provides The Direct Energy Bandgap Eg.

The constant A varies with different transitions denoted by n, where for direct transitions n takes values such as 1/2 or 2/3 and 2 or 3 for indirect transitions, depending on their permissibility[12]. Researchers commonly apply this formula to assess the bandgap of SnO_2 samples, consistently finding that SnO_2 exhibits a direct bandgap [13].

Bandgap determination involves plotting $(\alpha hv)^2$ against photon energy (*hv*), and enhanced linearity in these plots indicates a direct band transition. Extrapolating the linear section to $\alpha = 0$ yielded the bandgap value of the

samples as shown in Figure 5 [12]. The bandgap (E_g) values for the $Sn_{1-x}Sb_xO_{2-\delta}$ samples with antimony (Sb) concentrations x = 0.0, 0.1, 0.2 and 0.3 are 3.367 eV, 3.406 eV, 3.511 eV and 3.558 eV respectively. From Figure 5(a-d), it can be observed that the bandgap of the samples increases with the increase in concentration of Sb doping in SnO_2.

4. CONCLUSIONS

The Sb-doped SnO_2 ($Sn_{1-x}Sb_xO_2$) samples with x = 0.0, 0.1, 0.2, and 0.3 have been through standard ceramic methods. X-ray diffraction analysis confirmed crystalline tetragonal rutile phase, belonging to space group $P4_2/mnm$ (number 136). Slight increases in lattice parameters occurred with rising Sb content, likely due to differing ionic radii of Sb^{3+} (0.90 Å) ions and Sn^{4+} (0.72 Å). Undoped tin oxide exhibited a 67 nm grain size, closely packed with few pores. Antimony doping increased pore density. SEM and TEM images illustrated larger grain sizes in antimony-doped samples. Reflectance and transmittance increased, while absorbance decreased with higher Sb concentration. The energy bandgap rose from 3.367 to 3.558 eV with increasing Sb content. The enhancement in structural, Microstructural, optical properties results from an elevated lattice parameter and increased presence of oxygen vacancies.

REFERENCES

[1] L. Xiong, Y. Guo, J. Wen, H. Liu, G. Yang, P. Qin, G. Fang, Review on the Application of SnO_2 in Perovskite Solar Cells, Adv Funct Mater. 28 (2018) 1–18. https://doi.org/10.1002/adfm.201802757.

[2] A. Gaur, A. Kumar, P. Kumar, R. Agrawal, J. Shah, R.K. Kotnala, Fabrication of a SnO_2 - Based Hydroelectric Cell for Green Energy Production, ACS Omega. 5 (2020) 10240–10246. https://doi.org/10.1021/acsomega.9b03309.

[3] M. John Silvister Raju, S.S. Bhattacharya, Structural and optical properties of Sb doped SnO_2nanopowders synthesized by nebulizer spray pyrolysis, Mater Today Proc. 5 (2018) 10097– 10103. https://doi.org/10.1016/j.matpr.2017.11.005.

[4] K. Balasubramanian, G. Venkatachari, Synthesis and characterization of Sb doped SnO_2 forthe photovoltaic applications: Different route, Mater Res Express. 6 (2019). https://doi.org/10.1088/2053-1591/ab82c6.

[5] Y. Yang, Y. Wang, S. Yin, Oxygen vacancies confined in SnO_2 nanoparticles for desirable electronic structure and enhanced visible light photocatalytic activity, Appl Surf Sci. 420 (2017) 399–406. https://doi.org/10.1016/j.apsusc.2017.05.176.

[6] S. Saini, J. Shah, R.K. Kotnala, K.L. Yadav, Nickel substituted oxygen deficient nanoporouslithium ferrite based green energy device hydroelectric cell, J Alloys Compd. 827 (2020) 154334. https://doi.org/10.1016/j.jallcom.2020.154334.

[7] J. Shah, R. Kumar Kotnala, Rapid green synthesis of ZnO nanoparticles using a hydroelectric cell without an electrolyte, Journal of Physics and Chemistry of Solids. 108 (2017) 15–20. https://doi.org/10.1016/j.jpcs.2017.04.007.

[8] S. Somacescu, P. Osiceanu, J.M. Calderon-Moreno, A. Sackmann, C.E. Simion, A. Stănoiu,Mesopororous $Sn_{0.9}$-x$In_{0.1}$Cu x(I)$O_{2-\delta}$ gas sensors with selectivity to H_2S working under humid air conditions, Microporous and Mesoporous Materials. 197 (2014) 63–71. https://doi.org/10.1016/j.micromeso.2014.06.001.

[9] S.G. Lee, S.B. Han, W.J. Lee, K.W. Park, Effect of Sb-doped SnO_2 nanostructures on electrocatalytic performance of a Pt catalyst for methanol oxidation reaction, Catalysts. 10 (2020) 1–15. https://doi.org/10.3390/catal10080866.

[10] R. Zhang, K. Li, S. Ren, J. Chen, X. Feng, Y. Jiang, Z. He, L. Dai, L. Wang, Sb-doped SnO_2 nanoparticle-modified carbon paper as a superior electrode for a vanadium redox flow battery,Appl Surf Sci. 526 (2020). https://doi.org/10.1016/j.apsusc.2020.146685.

[11] K. Zawadzka, E. Godlewska, K. Mars, A. Kryshtal, A. Kruk, Interfacial stability of CoSb3 in contact with chromium: Reactive diffusion and microstructure evolution, J Alloys Compd. 843 (2020) 155862. https://doi.org/10.1016/j.jallcom.2020.155862.

[12] E. Karimi, S.M.B. Ghorashi, The Effect of SnO_2 and ZnO on the Performance of Perovskite Solar Cells, J Electron Mater. 49 (2020) 364–376. https://doi.org/10.1007/s11664-019-07804-4.

[13] J. Divya, A. Pramothkumar, S. Joshua Gnanamuthu, D.C. Bernice Victoria, P.C. Jobe prabakar, Structural, optical, electrical and magnetic properties of Cu and Ni doped SnO_2 nanoparticles prepared via Co-precipitation approach, Physica B Condens Matter. 588 (2020) 412169. https://doi.org/10.1016/j.physb.2020.412169